Published by
NIGERIAN SOCIETY OF PHYSICAL SCIENCES
Available online @ https://journal.nsps.org.ng/index.php/jnsps

J. Nig. Soc. Phys. Sci. 8 (2026) 2921

Journal of the Nigerian Society of Physical Sciences

Structural, electronic and optical properties of the $FeAs_{(1-x)}La_{(x)}$ ternary alloys: a first principles calculations

F. L. Kherfane[a], A. BOUKRAA[a], B. Beladel[b], A. Douara[c], I. E. Tibermacine[d], A. Rabehi[e], M. Benghanem[f,*]

[a]*Laboratory of New and Renewable Energy in Aride Zones (LENREZA), Kasdi Merbah University of Ouargla, Faculty of Mathematics and Material Sciences, BP. 511, 30 000 Ouargla, Algeria*
[b]*Ziane Achour University of Djelfa Faculty of the Exact Science and Computer Science BP.3117, 17 000 Djelfa Algeria*
[c]*Faculty of Science and Technology, Tissemsilt University, Tissemsilt, 38000, Algeria*
[d]*Department of Computer, Control, and Management Engineering, Sapienza University of Rome, 00185, Rome, Italy*
[e]*Telecommunications and Smart Systems Laboratory, University of Djelfa, PO Box 3117, Djelfa 17000, Algeria*
[f]*Physics Department, Faculty of Science, Islamic University of Madinah, Madinah, 42351, Saudi Arabia*

Abstract

This study investigates the structural, electronic, and optical properties of $FeAs_{(1-x)}La_{(x)}$ alloys $x = 0, 0.25, 0.5, 0.75, 1$ using the FP-LAPW method within the framework of density functional theory (DFT). The lattice parameter, bulk modulus, and its derivative were determined through Murnaghan's equation of state, revealing deviations from Vegard's law with increasing lanthanum concentration. Analysis of the electronic band structure and refractive indices highlights changes in the band gap, while energy-volume relationships indicate stability in the Zinc-Blende structure. Further exploration of the orthorhombic phase is suggested to confirm the structural properties. Doping FeAs with rare-earth elements introduces significant challenges due to disparities in ionic size, charge, and chemical behavior, yet it can profoundly impact structural, electronic, and superconducting properties such as charge carrier density and lattice parameters. The results emphasize the importance of precise control over doping concentrations and preparation techniques to achieve stable compounds. This theoretical work underscores the potential of FeAs-based materials for advanced applications, paving the way for further experimental validation.

DOI:10.46481/jnsps.2026.2921

Keywords: FP-LAPW, DFT, $FeAs_{(1-x)}La_{(x)}$, Ternary alloys, Superconductors, WIEN2K

Article History :
Received: 10 May 2025
Received in revised form: 30 June 2025
Accepted for publication: 15 July 2025
Published: 05 November 2025

© 2025 The Author(s). Published by the Nigerian Society of Physical Sciences under the terms of the Creative Commons Attribution 4.0 International license. Further distribution of this work must maintain attribution to the author(s) and the published article's title, journal citation, and DOI.

Communicated by: B. J Falaye

1. Introduction

The iron-arsenide-lanthanum $FeAs_{(1-x)}La_{(x)}$ alloys have attracted significant interest due to their promising applications in electronics and superconducting devices [1–5]. These alloys exhibit tunable electronic properties with varying lanthanum concentration, making them suitable for diverse applications [6]. They are characterized by high electron mobility, low carrier concentration, and good thermal stability, which make them ideal for advanced technologies such as superconductors and electronic sensors [7–10]. The current research focuses on investigating their structural, electronic, optical, thermodynamic, and elastic properties using first-principles calculations, aiming to understand their potential in advanced optical and electronic devices [11–14]. Over the past two decades, high-temperature

*Corresponding author Tel. No.: +966-50-734-6783
Email address: mbenghanem@iu.edu.sa (M. Benghanem)

superconductivity in copper oxides captured significant scientific interest and spurred extensive research. More recently, the discovery of superconductivity in iron-based pnictide oxides has similarly attracted attention. In February 2008, researchers from the Tokyo Institute of Technology revealed that fluorine-doped lanthanum oxide iron arsenide LaFeAsOF exhibited superconductivity at 24 K [15]. Subsequent studies quickly improved the critical temperature (Tc) by substituting lanthanum with other rare-earth elements. For instance, replacing La with cerium raised Tc to 41 K, while samarium substitution further increased it to 55 K. These rapid advancements demonstrated the potential of rare-earth doping to significantly enhance the superconducting properties of iron-based materials. Lanthanum from the rare earth family was selected to be added to the FeAs compound from the 111 structural type to explore the properties of the ternary compound and identify its potential applications [16, 17]. The study investigates the structural, electronic, and optical properties of $FeAs_{(1-x)}La_{(x)}$ alloys using DFT. Stability in the Zinc-Blende structure is suggested by energy-volume behavior, but further exploration in the orthorhombic structure is necessary. Proper doping significantly impacts structural, electronic, and superconducting properties, highlighting the potential of these compounds.

2. Calculation method

The calculations were performed using the FP-LAPW method to solve the Kohn–Sham equations self-consistently within Density Functional Theory (DFT) using the WIEN2k software [18]. Three different exchange-correlation approximations were employed: LDA, PBE-GGA, and WC-GGA, to compare structural properties [19]. It was observed that the GGA overestimates the lattice parameter and underestimates the band gap, while the LDA underestimates both the lattice parameter and the band gap but overestimates the bulk modulus. In contrast, the WC-GGA results fall between those of LDA and GGA [20–23]. However, all these approximations significantly underestimate the band gap. Meanwhile, the improved TB-mBJ approach has been shown to calculate electronic properties with greater accuracy, as in [24, 25]. For the electronic and optical calculations, denser k-point meshes were used, consisting of 2000 K points for the binary compounds and 50 K-points for the ternary alloys [26]. Furthermore, the inner shell electrons of Fe, As, and La were distinguished from their valence electrons. The iron Fe atom has an inner-shell configuration of ($1s^2$ $2s^2$ $2p^6$ $3s^2$ $3p^6$) and a valence configuration of ($4s^2$ $3d^6$). The arsenic As atom has an inner-shell configuration of ($1s^2$ $2s^2$ $2p^6$ $3s^2$ $3p^6$ $3d^{10}$) and a valence configuration of ($4s^2$ $4p^3$). Lastly, the lanthanum (La) atom has an inner-shell configuration of ($1s^2$ $2s^2$ $2p^6$ $3s^2$ $3p^6$ $5s^2$ $3d^{10}$ $4s^2$ $4p^6$ $4d^{10}$ $5s^2$ $5p^6$) and a valence configuration of ($5d^1$ $6s^2$).

3. Structural properties

The equilibrium structural parameters of the $FeAs_{(1-x)}La_{(x)}$ ternary alloys in the zinc-blende (ZB) structure, including the lattice parameter (a), bulk modulus (B) and its pressure derivative (B'), were determined by fitting the total energy versus volume to Murnaghan's equation of state (EOS) [27], as shown in Figure 1.

Table 1 summarizes the calculated structural parameters of the examined alloys, using both PBE GGA, WC-GGA and PW-LDA techniques. The obtained results are in good agreement with theoretical data [28].

The lattice parameter (a) increases with the rising concentration of lanthanum (La) in the alloys, ranging from 5.2607 Å for FeAs to 5.7774 Å for FeLa, indicating a significant expansion of the crystal lattice due to the larger atomic size of lanthanum [11, 12]. In contrast, the bulk modulus (B) and its derivative (B') decrease with increasing lanthanum content, reflecting a reduction in material stiffness [5, 29]. For instance, in the PBE-GGA method, the bulk modulus decreases from 116.7933 GPa for FeAs to 38.8606 GPa for FeLa. Additionally, the PW-LDA method shows notable differences, recording higher bulk modulus values at certain La concentrations, which may require further verification of its accuracy. The results highlight how composition affects mechanical properties, as the alloys become less rigid with more lanthanum, indicating changes in atomic bonding. Variations of the lattice constant and bulk modulus versus the La concentration x for the ZB $FeAs_{(1x)}La_{(x)}$ are plotted in Figure 2.

Figure 2 illustrates the relationship between the composition xx of the $FeAs_{(1-x)}La_{(x)}$ compound and the lattice parameter across different computational methods. The data show a general increase in the lattice parameter as the value of xx rises, indicating that the introduction of lanthanum (La) into the FeAs structure leads to an expansion of the crystal lattice due to the larger atomic size of La. The three computational methods PBE-GGA, WC-GGA, and PW-LDA yield different results, with PBE GGA giving the highest lattice parameters, PW-LDA the lowest while WC method provides intermediate values. The lattice parameter ranges from 5.232 Å for FeAs at $x = 0$ to 5.464 Å for FeLa at $x = 1$ using PBE-GGA. These trends suggest that increasing lanthanum content expands the lattice, potentially affecting the electronic, magnetic, and optical properties of the material. Figure 3 shows that as Lanthanum (La) concentration increases in the $FeAs_{(1-x)}La_{(x)}$ compound, the $FeAs_{(1-x)}La_{(x)}$The PBE-GGA method yields the highest bulk modulus values, while PW-LDA gives the lowest, especially at higher La concentrations. The most significant decrease occurs when transitioning from pure FeAs ($x = 0$) to $FeAs_{75}La_{25}$ ($x = 0.75$), where the bulk modulus drops from 116 GPa to 53 GPa. These trends suggest that the mechanical properties of the compound can be adjusted by varying the composition, which is useful for applications in superconductivity and structural materials.

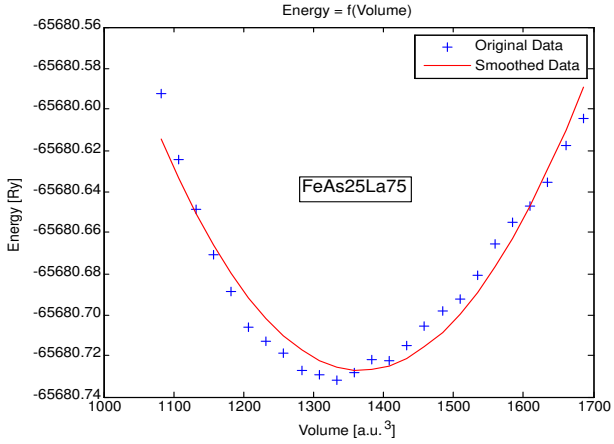

(a)

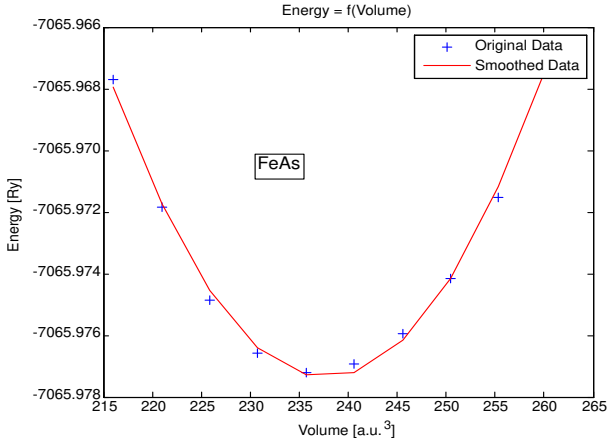

(b)

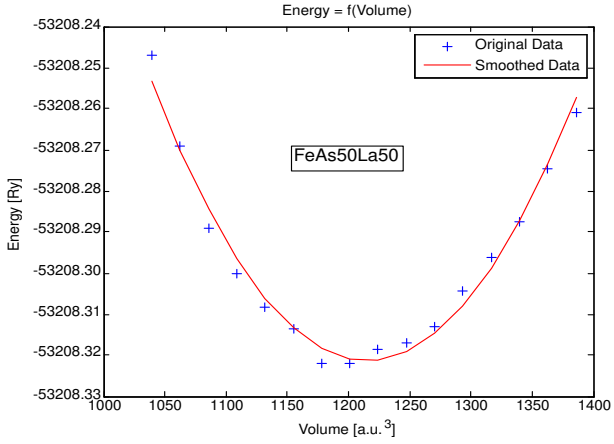

(c)

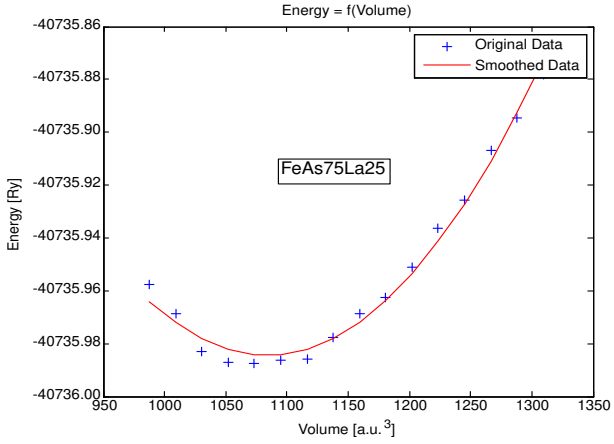

(d)

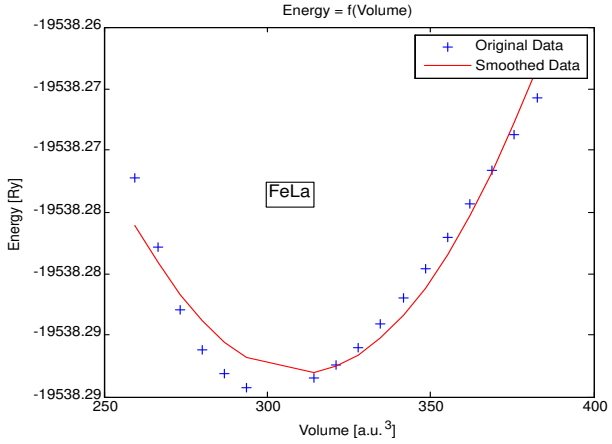

(e)

Figure 1: Energy versus the volume at equilibrium of the $FeAs_{(1-x)}La_{(x)}$ for the concentrations (a) x=0, (b) x=1, (c) x=0.25, (d) x=0.5 and (e) x=0.75 from WC-GGA.

Table 1: Comparison of lattice parameter a, bulk modulus B, and its derivative B' for different methods.

Methods	PBE-GGA			WC-GGA			PW-LDA		
Parameters	a(A°)	B(GPa)	B'	a(A°)	B(GPa)	B'	a(A°)	B(GPa)	B'
FeAs	5.2607	116.7933	3.9532	5.2002	141.0037	1.1059	5.1442	142.8474	4.7837
$FeAs_{75}La_{25}$	5.4990	87.0610	5.7166	5.4254	100.7044	5.6940	5.3661	137.5969	8.3214
$FeAs_{50}La_{50}$	5.7099	64.6193	5.2027	5.6259	78.0434	3.8479	5.5526	84.0881	4.8472
$FeAs_{25}La_{75}$	5.9215	53.0414	4.1704	5.8155	59.9155	4.7642	5.7345	66.6649	4.7676
FeLa	5.7774	38.8606	5.8721	5.6331	60.2253	6.7472	5.5357	77.8563	8.4735

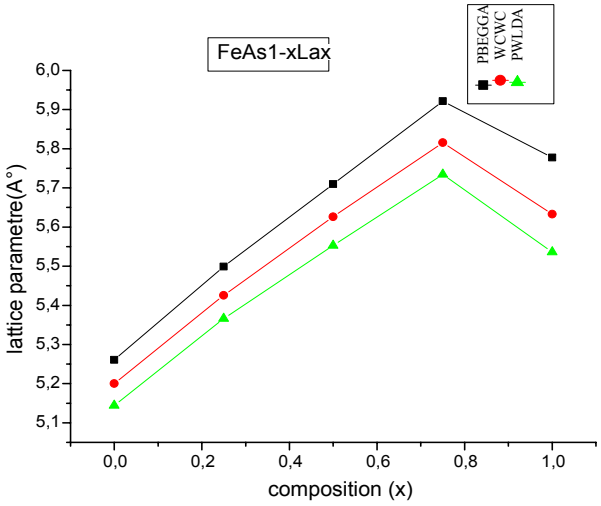

Figure 2: Variation of the lattice constant versus composition, x of the $FeAs_{(1-x)}La_{(x)}$.

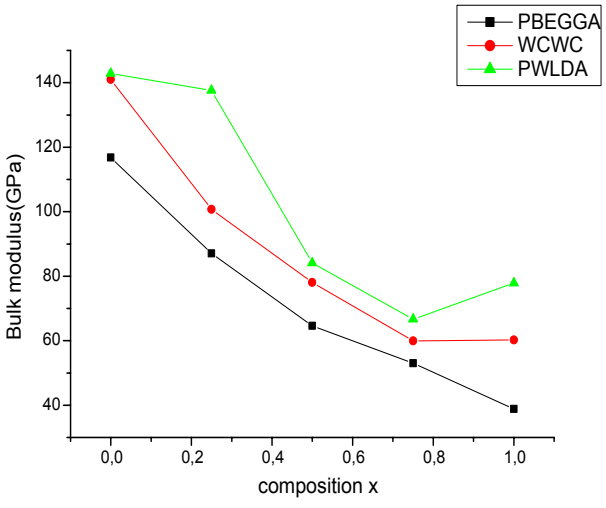

Figure 3: Variation of the bulk modulus versus composition, x of the $FeAs_{(1-x)}La_{(x)}$ alloy.

4. Electronic properties

The electronic band structure and density of states (DOS) of the $FeAs_{(1-x)}La_{(x)}$ alloy are investigated. The band structure energies calculated using the PBE-GGA approach indicated a direct band gap positioned at the gamma Γ symmetry point in the range of the concentration, $x = 0.00, 0.25, 0.50, 0.75$ [14] [30]. The band gap energies calculated using the PBE-GGA, WC- GGA and PW-LDA approximations for the binary FeAs, FeLa compounds and their ternary $FeAs_{(1-x)}La_{(x)}$ alloy are listed in Table 2.

This table analyzes the total energy and energy differences between various states for FeAs and its lanthanum (La) alloys using PBE, WC, and LDA methods. FeAs has the highest energy values, indicating its stability. As lanthanum is added, the total energy and energy differences decrease, reflecting changes in electronic and bonding properties. WC and LDA methods give slightly higher energy values than PBE, but all three methods provide reliable results. Energy differences between states decrease with increasing La content, but the (γ) state remains more stable than the x state. These findings suggest that introducing lanthanum modifies the energetic properties of the alloys . On the other hand, the variations of the direct and indirect band gaps energies with concentration x for the $FeAs_{(1-x)}La_{(x)}$ compound are illustrated in Figure 4.

5. Density of states

Figure 5 illustrate the total density of states (DOS) shows significant peaks at 0 eV and 4 eV, indicating a high density of available electronic states at these levels. The main contributors to the DOS are the electronic states from the 1d sublevel of iron (Fe) and the 2d sublevel of lanthanum (La), which play a key role in the material's electronic properties [6] [29]. In contrast, the contributions from the 1s and 2s sublevels are minimal, suggesting they have little impact on the electronic characteristics of the material.

Figure 6. Illustrate the total density of states (DOS), and shows significant peaks at 0 eV and 4 eV, indicating a high density of electronic states at these levels. The main contributors to the DOS are the 1d sublevel of iron (Fe) and the 2d sublevel of lanthanum (La), which significantly shape the material's electronic properties. In contrast, the contributions from the 1s and 2s sublevels are minimal, suggesting that they have little effect on the electronic characteristics of the material.

Table 2: Band gap energies of binary compounds FeAs, FeLa and ternary $FeAs_{(1-x)}La_{(x)}$ alloys.

Energy (e.V)	$E_{\gamma-\gamma}$ (e.v)			$E_{\gamma-x}$ (e.v)		
Methods	PBE	WC	LDA	PBE	WC	LDA
FeAs	0.99427	1.00583	1.00583	1.62630	1.64522	1.64522
FeAs75La25	0.52363	0.53074	0.53660	0.82595	0.83716	0.84641
FeAs50La50	0.50429	0.51182	0.51182	0.79545	0.80732	0.80732
FeAs25La75	0.48627	0.49514	0.50213	0.76702	0.78100	0.79203
FeLa	0.90534	0.92854	0.94487	1.48085	1.511878	1.54550

The electronic activity is mainly concentrated between -2 and 3 eV, with a peak at 1 eV and a density around 5. Iron shows significant activity between 0 and 2 eV, with a peak at 2 eV and a density of about 4, indicating its key role near the Fermi level. Arsenic exhibits a broader activity range from -4 to 4 eV, with a peak at 2 eV. Lanthanum has limited activity, mostly between 0 and 3 eV, with a peak at 2 eV and a density of up to 1.5. These findings suggest metallic or conductive behavior, driven primarily by iron and arsenic, with a minor contribution from Lanthanum as mentioned in Figure 7.

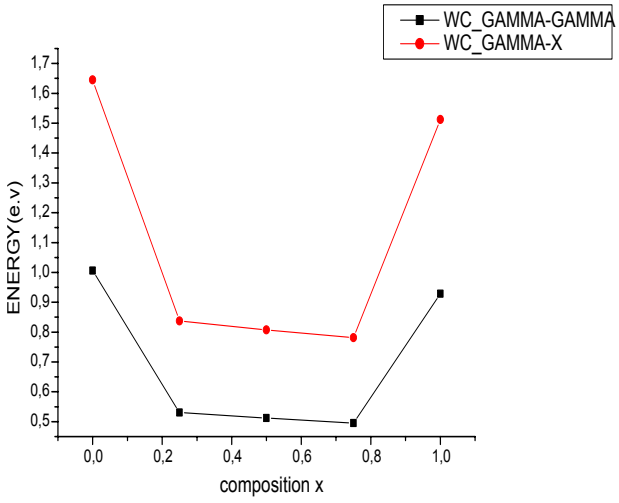

Figure 4: Direct and indirect band gap energies as function of composition of the ternary alloy $FeAs_{(1-x)}La_{(x)}$.

6. Optical properties

The comparison of the real part of the dielectric constant ($\epsilon 1$) for FeAs and FeLa reveals distinct behaviors over an energy range up to 14 eV. FeAs shows a strong peak at 11 eV, reaching 75 eV, indicating a robust ability to store electric energy, while FeLa has a weaker peak below 50 in the same region. In the mid-energy range (22 eV to 88 eV) , both materials experience a sharp decline in $\epsilon 1$ values, approaching zero at times, with FeLa maintaining relatively higher values, reflecting differences in electronic structures. Beyond 88 eV, $\epsilon 1$ stabilizes near zero for both materials, indicating minimal response to electric fields.

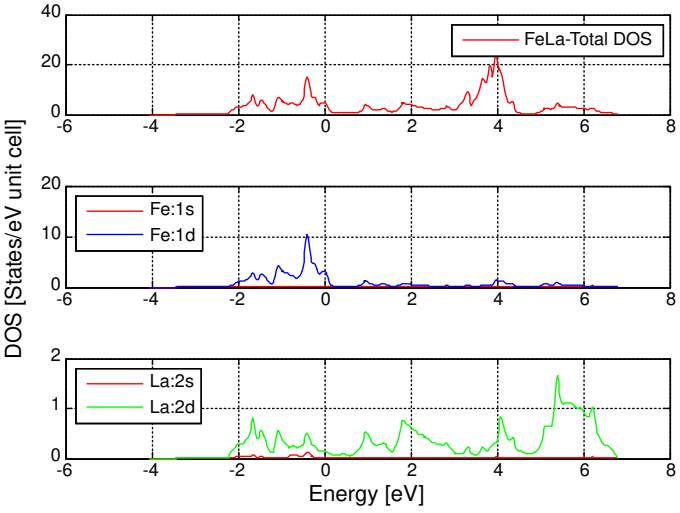

Figure 5: Total and partial DOS of FeAs.

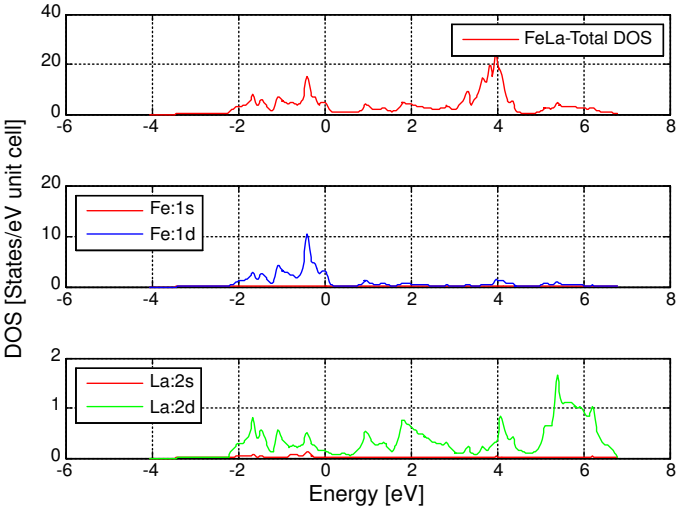

Figure 6: Total and partial DOS of $FeAs_{75}La_{25}$.

FeAs is well-suited for energy storage or low-frequency applications due to its strong low-energy response, while FeLa broader stability favors applications requiring diverse energy

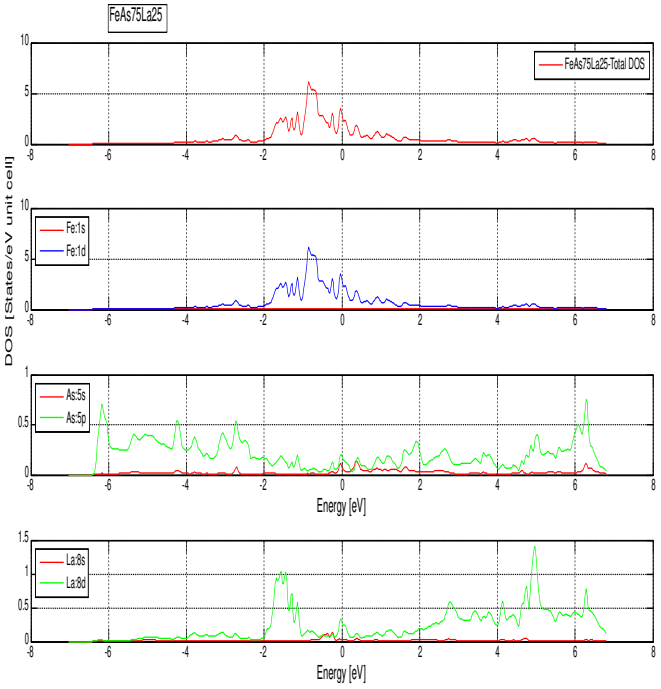

Figure 7: Total and partial DOS of FeLa.

ranges. These results (Figure 8) highlight the need for further study on the effects of thermal and pressure conditions to better understand the dynamic properties of these materials.

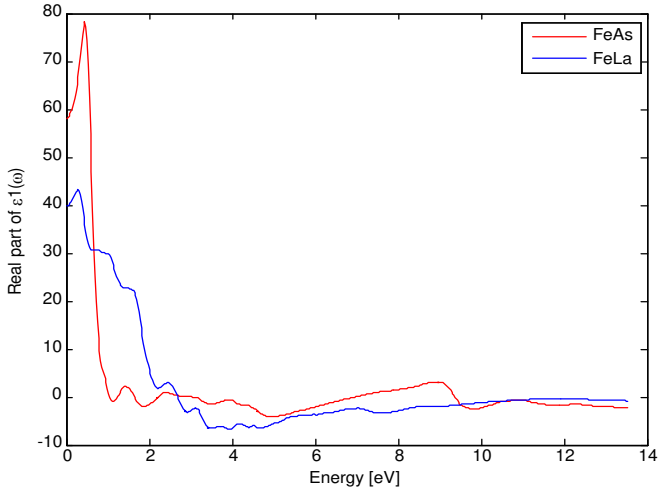

Figure 8: Real parts of binary FeAs and FeLa compound.

The Figure 9 compares the dielectric properties ($\epsilon 2$) of FeAs and FeLa over an energy range up to 14 eV. FeAs shows a strong peak at 11 eV, indicating concentrated electronic transitions, while FeLa displays more dispersed behavior with less distinct peaks. In the mid-energy range 22 eV to 88 eV, FeLa exhibits more complex features with multiple small peaks, whereas FeAs remains stable. At higher energies (above 88 eV), both materials show a gradual decrease in $\epsilon 2$, with FeLa maintaining slightly higher values.

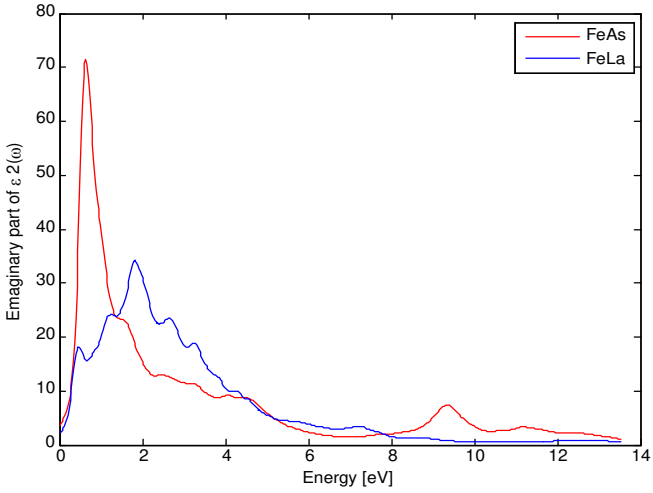

Figure 9: Imaginary parts of binary FeAs and FeLa compound.

FeAs demonstrates high absorption at low energies, making it suitable for electronic absorption applications, while FeLa broader absorption range favors applications requiring extended energy responses. These differences arise from their distinct electronic structures. Further studies are recommended to optimize their use in electronics and photonics [31] [32].

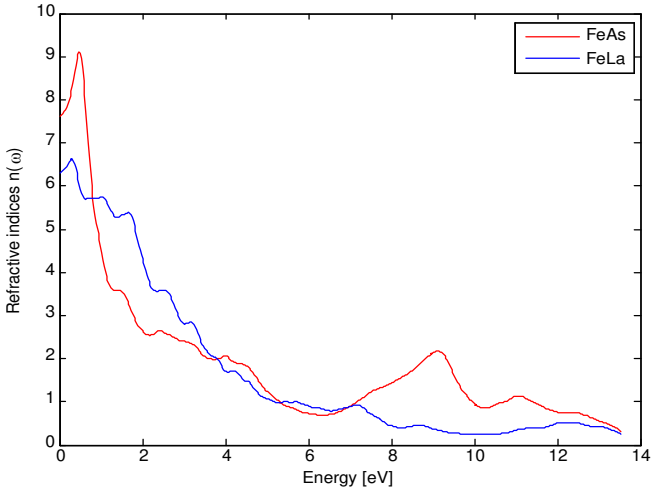

Figure 10: Refractive indices of binary FeAs and FeLa compound.

The Figure 10 compares the refractive index (n) of FeAs and FeLa over an energy range up to 14 eV. At low energies,

both materials have high refractive indices, with FeAs reaching around 9 and FeLa around 8 at 11 eV, indicating FeAs has a stronger ability to slow light. Between 22 and 88 eV, both materials show a gradual decrease in the refractive index, with

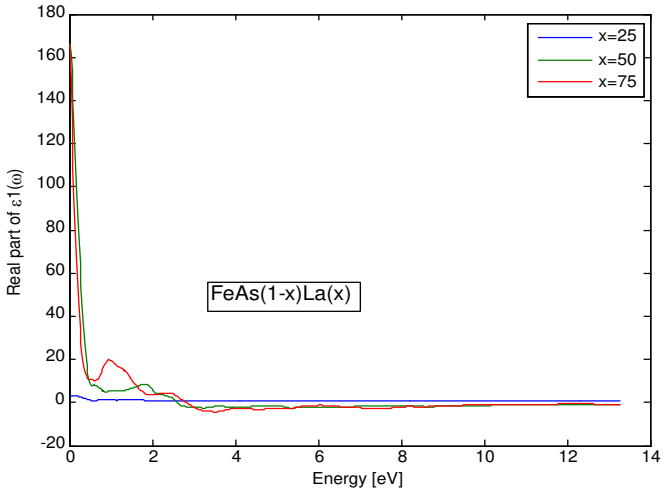

Figure 11: Real parts of ternary $FeAs_{(1-x)}La_{(x)}$ where: x=0.25,0.50 and 1.

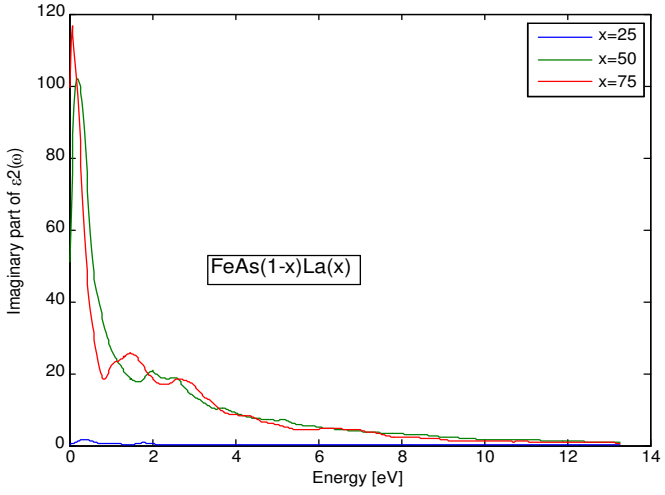

Figure 12: Real parts of ternary $FeAs_{(1-x)}La_{(x)}$ where: x=0.25,0.50 and 1.

FeAs maintaining higher values, reflecting a stronger optical response. Above 88 eV, both materials' refractive indices approach zero, indicating a weakened effect.

One can conclude that FeAs is more suitable for applications requiring control over light speed or reduced optical losses, while FeLa stable decrease makes it better for applications needing consistent optical properties across a wide energy range.

Figure 11 shows the relationship between the real part of the dielectric constant ($\epsilon 1$) and energy for the compound $FeAs_{(1-x)}La_{(x)}$ at different concentrations of La ($x = 25, 50, 75$). At low energies (< 2 eV), the dielectric constant is high but rapidly decreases as energy increases, with the curves converging and approaching zero after 2 eV. The dielectric constant at low energies is lower for the $x = 25$ curve compared to $x = 75$, indicating the effect of chemical composition on the material's response.

The high dielectric constant at low energies may be due to conduction or ionization effects, while the stability at higher energies suggests that the valence electrons are no longer impacted. The Lanthanum concentration significantly influences electrical properties, potentially enhancing conductivity or altering the electronic structure.

Figure 12 illustrates the imaginary part of the dielectric function (ϵ_2) for $FeAs_{(1-x)}La_{(x)}$ at different lanthanum concentrations (x =25%, 50% and 75%). It shows that as lanthanum concentration increases, the dielectric function decreases, especially at higher energies (2-4 eV). The peak near 0 eV, indicative of electronic transitions near the Fermi level, decreases in magnitude and shifts with higher lanthanum content. At x = 25%, electronic activity is highest, while at x = 75%, it is lowest, suggesting that lanthanum incorporation reduces electronic activity. These findings imply that lanthanum substitution alters the electronic properties of the material, which may be relevant for optoelectronics or superconductivity.

The Figure 13 shows the relationship between the refractive index (n) and energy for $FeAs_{(1-x)}La_{(x)}$ at different La concentrations ($x = 25, 50, 75$). At low energies (< 2 eV), the refractive index is higher, especially for $x = 50$ and 75, indicating stronger light interaction. The $x = 25$ curve shows lower values, highlighting the impact of chemical composition on light propagation. As energy increases, the refractive index decreases for all concentrations, with the material becoming less interactive with light. These findings are important for applications requiring refractive index control, such as optical coatings and anti-reflective materials [26] [33].

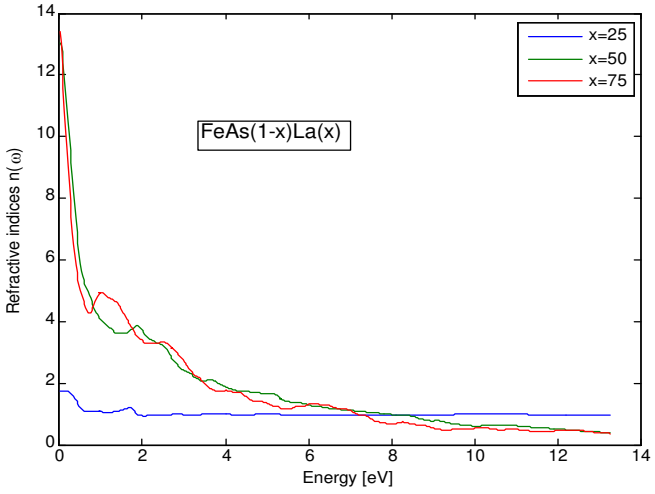

Figure 13: Refractive indices of ternary alloys $FeAs_{(1-x)}La_{(x)}$ for compositions (x = 0.25, 0.5 and 0.75).

7. Conclusion

This theoretical study investigated the feasibility of doping the FeAs compound with rare-earth elements of the 111 structural type, aiming to achieve a stable compound with novel superconducting or magnetic properties. The findings demonstrated the stability of the $FeAs_{(1-x)}La_{(x)}$ system with a zinc-blende structure. Incorporating lanthanum, due to its larger atomic size, results in an expansion of the crystal lattice, significantly affecting the material's physical properties. These modifications are particularly relevant for potential applications in fields such as superconductivity and magnetism. Additionally, the study highlighted the critical role of computational methods in accurately characterizing the structure and mechanical properties of these materials. The observed differences between methods underscore the importance of selecting appropriate techniques to ensure reliable results for future research and applications.

The impact of lanthanum doping on the lattice parameter, specifically the expansion caused by larger "La" atoms, provides valuable insights for future studies focusing on the physical properties and technological applications of FeAs-based materials. Notably, for $FeAs_{(1-x)}La_{(x)}$ compositions (x = 0.25, 0.5, and 0.75), no prior theoretical or experimental data are available, making this study the first to predict their properties.

Looking ahead, exploring this system in an orthorhombic structure is recommended to identify the most stable configuration and to deepen the understanding of its structural, electronic, and mechanical properties.

Acknowledgements

The researchers wish to extend their sincere gratitude to the Deanship of Scientific Research at the Islamic University of Madinah (KSA) for the support provided to the Post-Publishing Program.

References

[1] H. Kaur, H. Kaur & A. Sharma, "A review of recent advancement in superconductors", Mater Today Proc **37** (2021) 3612. https://doi.org/10.1016/j.matpr.2020.09.771.

[2] A. Douara, A. Rabehi, M. Guermoui, R. Daha & I. E. Tibermacine, "Impact of AlN Buffer Layer Thickness on Electronic and Electrical Characteristics of In0.17Al0.83N/GaN High-Electron-Mobility Transistor", Physics of the Solid State **66** (2024) 157. https://doi.org/10.1134/S1063783424600766.

[3] A. Rabehi, A. Douara, M. Elbar, R. Zenzen & M. Amrani, "Impact of Grain Boundaries on The Electrical Characteristics and Breakdown Behavior of Polycrystalline Silicon Pin Diodes: A Simulation Study, ITEGAM-JETIA", **10** (2024) 59. https://doi.org/10.5935/jetia.v10i49.1196.

[4] A. Douara, A. Rabehi, M. Guermoui, R. Daha & I.E. Tibermacine, "Simulation-based optimization of barrier and spacer layers in InAlN/GaN HEMTs for improved 2DEG density, Micro and Nanostructures", **195** (2024) 207950. https://doi.org/10.1016/j.micrna.2024.207950.

[5] J. E. Moore, "The birth of topological insulators" Nature **464** (2010) 194. https://doi.org/10.1038/nature08916.

[6] P. Li & H. Li, "Recent progress in the lanthanide-complexes based luminescent hybrid materials", Coord Chem Rev **441** (2021) 213988. https://doi.org/10.1016/j.ccr.2021.213988.

[7] J. Wang, L. Huang, S. Lin, S. Xu & G. Bai, "Lanthanide doped semiconductor thin films for photonic and optoelectronic applications", Appl Phys Rev **12** (2025). https://doi.org/10.1063/5.0220910.

[8] A. Rabehi, A. Douara, A. Rabehi, H. Helal, A. M. Younsi, M. Amrani, I. E. Abbas, E. Comini & Z. Benamara, "Accurate parameter estimation of Au/GaN/GaAs schottky diode model using grey wolf optimization", Revista Mexicana de Física **70** (2024). https://doi.org/10.31349/RevMexFis.70.021004.

[9] A. Douara, A. Rabehi & O. Baitiche, "Impact of AlN interlayer on the electronic and I-V characteristics of In0.17Al0.83N/GaN HEMTs devices", Revista Mexicana de Física **69** (2023). https://doi.org/10.31349/RevMexFis.69.031602.

[10] H. Hafiz, A. I. Khair, H. Choi, A. Mueen, A. Bansil, S. Eidenbenz, J. Wills, J. X. Zhu, A. V. Balatsky & T. Ahmed, "A high-throughput data analysis and materials discovery tool for strongly correlated materials", NPJ Comput Mater **4** (2018) 63. https://doi.org/10.1038/s41524-018-0120-9.

[11] R. Moussa, A. Abdiche, R. Khenata, X. T. Wang, D. Varshney, X. W. Sun, S. Bin Omran, A. Bouhemadou & D. P. Rai, "Structural, electronic, optical, thermodynamic and elastic properties of the zinc-blende $Al_xIn_{1-x}N$ ternary alloys: A first principles calculations", Journal of Physics and Chemistry of Solids **119** (2018) 36. https://doi.org/10.1016/j.jpcs.2018.03.035.

[12] A. Douara, A. Rabehi, O. Baitiche & M. Handami, "Improved electrical characteristics of AlxGa1-xN/GaN High Electron Mobility Transistor by effect of physical and geometrical parameters", Revista Mexicana de Física **69** (2023) 4. https://doi.org/10.31349/RevMexFis.69.041001.

[13] G. Kresse & J. Hafner, "Ab initio molecular dynamics for liquid metals", Phys Rev B **47** (1993) 558. https://doi.org/10.1103/PhysRevB.47.558.

[14] O. Slobodyan, J. Flicker, J. Dickerson, J. Shoemaker, A. Binder, T. Smith, S. Goodnick, R. Kaplar & M. Hollis, "Analysis of the dependence of critical electric field on semiconductor bandgap", J Mater Res **37** (2022) 849. https://doi.org/10.1557/s43578-021-00465-2.

[15] Y. Kamihara, T. Watanabe, M. Hirano & H. Hosono, "Iron-Based Layered Superconductor $La[O_{1-x}F_x]FeAs$ (x = 0.05 - 0.12) with Tc = 26 K", J Am Chem Soc **130** (2008) 3296. https://doi.org/10.1021/ja800073m.

[16] A. Ziane, A. Rabehi, A. Rouabhia, M. Amrani, A. Douara, R. Dabou, A. Necaibia, M. Mostefaoui & N. Sahouane, "Numerical Investigation of G–V Measurements of metal – a Nitride GaAs junction", Revista Mexicana de Física **70** (2024). https://doi.org/10.31349/RevMexFis.70.061604.

[17] J. Paglione & R. L. Greene, "High-temperature superconductivity in iron-based materials", Nat Phys **6** (2010) 645. https://doi.org/10.1038/nphys1759.

[18] K. Schwarz & P. Blaha, "Solid state calculations using WIEN2k", Comput Mater Sci **28** (2003) 259. https://doi.org/10.1016/S0927-0256(03)00112-5.

[19] J. Heyd, G.E. Scuseria & M. Ernzerhof, "Hybrid functionals based on a screened Coulomb potential", J Chem Phys **118** (2003) 8207. https://doi.org/10.1063/1.1564060.

[20] F. Tran & P. Blaha, "Accurate Band Gaps of Semiconductors and Insulators with a Semilocal Exchange-Correlatiohn Potential", Phys Rev Lett **102** (2009) 226401. https://doi.org/10.1103/PhysRevLett.102.226401.

[21] A. Rabehi, A. Rabehi, A. Douara, H. Helal, O. Baitiche, B. Akkal, M. Amrani, S. Tizi & Z. Benamara, "Modeling the Abnormal Behavior of the 6H-SiC Schottky Diode Using Lambert W Function", Journal of Nano- and Electronic Physics **14** (2022) 06032. https://doi.org/10.21272/jnep.14(6).06032.

[22] A. Douara, A. Rabehi, B. Djellouli, A. Ziane & H. Abid, "2-D optimisation current–voltage characteristics in AlGaN/GaN HEMTs with influence of passivation layer", International Journal of Ambient Energy **42** (2021) 1363. https://doi.org/10.1080/01430750.2019.1608856.

[23] H. Jin, D.J. Blackwood, Y. Wang, M.-F. Ng & T.L. Tan, "First-principles study of surface orientation dependent corrosion of BCC iron", Corros Sci **196** (2022) 110029. https://doi.org/10.1016/j.corsci.2021.110029.

[24] P. Huang & E. A. Carter, "Advances in Correlated Electronic Structure Methods for Solids, Surfaces, and Nanostructures", Annu Rev Phys Chem **59** (2008) 261. https://doi.org/10.1146/annurev.physchem.59.

032607.093528.

[25] Y. Huang, C. Yu, W. Chen, Y. Liu, C. Li, C. Niu, F. Wang & Y. Jia, "Band gap and band alignment prediction of nitride-based semiconductors using machine learning", J Mater Chem C Mater **7** (2019) 3238. https://doi.org/10.1039/C8TC05554H.

[26] W. S. Ko, K. B. Park & H. -K. Park, "Density functional theory study on the role of ternary alloying elements in TiFe-based hydrogen storage alloys", J Mater Sci Technol **92** (2021) 148. https://doi.org/10.1016/j.jmst.2021.03.042.

[27] F. D. Murnaghan, "The Compressibility of Media under Extreme Pressures", Proceedings of the National Academy of Sciences **30** (1944) 244. https://doi.org/10.1073/pnas.30.9.244.

[28] J. S. Wróbel, D. Nguyen-Manh, M.Y. Lavrentiev, M. Muzyk & S. L. Dudarev, "Phase stability of ternary fcc and bcc Fe-Cr-Ni alloys", Phys Rev B **91** (2015) 024108. https://doi.org/10.1103/PhysRevB.91.024108.

[29] R. W. Boyd, A. L. Gaeta & E. Giese, *Nonlinear Optics*, Springer, Cham, 2023, pp. 1097–1110. https://doi.org/10.1007/978-3-030-73893-8_76.

[30] S. Grimme, "Density functional theory with London dispersion corrections", WIREs Computational Molecular Science **1** (2011) 211. https://doi.org/10.1002/wcms.30.

[31] M. A. Green, A. Ho-Baillie, H. J. Snaith, "The emergence of perovskite solar cells", Nat Photonics **8** (2014) 506. https://doi.org/10.1038/nphoton.2014.134.

[32] T. Qu, M. Wang, X. Cheng, X. Cui, R. Y. Zhang, Z. Q. Zhang, L. Zhang, J. Chen & C. T. Chan, "Topological Photonic Alloy", Phys Rev Lett **132** (2024) 223802. https://doi.org/10.1103/PhysRevLett.132.223802.

[33] H. C. L. Tsui & N. Healy, "Recent progress of semiconductor optoelectronic fibers", Frontiers of Optoelectronics **14** (2021) 383. https://doi.org/10.1007/s12200-021-1226-0.